Heat Transfer

WILEY

HEAT TRANSFER

ORIGINAL ARTICLE OPEN ACCESS

Perspective Projection of an Ellipse and an Ellipsoid for Analytical View Factor Evaluation

Kaname Sasaki

Institute of Space Systems, German Aerospace Center (DLR), Bremen, Germany

Correspondence: Kaname Sasaki (kaname.sasaki@dlr.de)

Received: 27 March 2025 | **Revised:** 1 May 2025 | **Accepted:** 21 May 2025

Keywords: ellipse | ellipsoid | perspective projection | radiative heat transfer | view factor

ABSTRACT

Radiative view factors are fundamental quantities for evaluating radiative heat transfer between different surfaces. While analytical expressions of view factors have been evaluated for various types of basic geometries, including circular disks and spheres, extending these solutions to more complex geometries, such as ellipses and ellipsoids has remained challenging due to mathematical complexity. This study evaluates the analytical view factor expressions of an ellipse and a triaxial ellipsoid from a plate element in an arbitrary position and orientation. The proposed analytical methods generalize the existing analytical solutions for disk and sphere related geometries, and extend their applicability to more complex geometrical configurations. For both cases, the perspective projection of the target geometry is analyzed, and the original view factor is transformed into an equivalent ellipse view factor, which has known analytical solutions from the previous study. Finally, the derived view factor expressions are validated by comparison with the numerical results.

1 | Introduction

Radiative view factors are the fundamental quantities in the field of radiative heat transfer. This parameter quantifies radiative heat exchange between different surfaces based on the assumptions of Lambertian radiation and reflection. The derivation of analytical view factors is challenging due to the integration complexity. Even for simple geometries, such as triangular polygons or rectangular plates, the analytical evaluation of view factors is highly complicated [1–3]. Nevertheless, view factors for various types of geometries have been investigated in the past studies, and the collection of analytical view factor solutions were compiled by Howell and Mengüç [4] and Howell [5].

View factors of circular disks and spheres are applied in different fields, such as the evaluation of fireball thermal radiation from flammable fuels [6, 7], lighting and heat transfer evaluation in the civil engineering field [8, 9], and heat flux analysis for earth-orbiting spacecraft [10, 11]. Analytical solutions of view factors between a disk and various geometries, such as a plate element, a disk, a spheroid, and a paraboloid, were investigated in the past studies [12–15]. Similarly, investigations on the view factors between a sphere and different types of geometries were performed in the series of studies conducted by Chung and Naraghi [16, 17] and Sabet and Chung [18]. Also, the view factor of a part of a sphere from a plate element has been investigated as well [19, 20].

Extending the disk and sphere view factors to elliptical and ellipsoidal shapes is expected to be useful for further applications. For example, thermal radiation from a jet fire is commonly modeled as a combination of conical, cylindrical, and ellipsoidal shapes [21–23]. For evaluating the thermal radiation and shadowing of crops and plants, the related geometry can be modeled as spheroidal shapes [24–27], In addition, in the field of aerospace engineering, application examples can be found in evaluating the radiative heat exchange of aerostats [28–30], and the thermophysical modeling of the binary asteroid: 65803 Didymos system [31]. However,

the available analytical solutions were limited to some specific cases for an ellipse [32, 33] and a spheroid [12, 17], due to the significantly increased complexity in the calculation. In the recent study by Sasaki [34], view factors of an ellipse from a plate element were derived, where the plate element is placed on the normal line passing through the ellipse center as shown in Figure 1. Additionally, view factors of a spheroid from a plate element were evaluated, based on its axisymmetric characteristics. Although these solutions extended the applicable geometrical configurations, the ellipse view factor from a plate element in an arbitrary position and orientation, and the triaxial ellipsoid view factor from a plate element remained unsolved.

In this study, the analytical view factor expressions for the generalized cases: ellipse and triaxial ellipsoid from a plate element in an arbitrary position and orientation, are evaluated. For both cases, the perspective projection of the target geometry is considered, and the original view factor is transformed into an equivalent ellipse view factor, where the analytical solutions are available (Figure 1). The transformation process employed in this study is analogous to the methodology of the analytical solid angle evaluation for an ellipse and ellipsoid from a point source, presented by Conway [35] and Heitz [36, 37].

The solid angle between two differential areas from dA_i to dA_j is given by Equation (1), and the view factor for the same configuration is given by Equation (2). The related geometrical configuration is presented in Figure 2.

$$d\Omega = \frac{dA_j \cos\theta_j}{S^2}, \tag{1}$$

$$dF = \frac{dA_j \cos\theta_i \cos\theta_j}{\pi S^2}. \tag{2}$$

Apart from the normalization coefficient, the major difference between the solid angle and the view factor is the angular dependency with respect to the radiation source. View factor assumes the Lambertian distribution from the surface, while the solid angle corresponds to the homogeneous distribution from a point source. For the radiative heat transfer evaluation, the view factor is typically the relevant quantity. However, in the field of nuclear and radiation technologies, the solid angle is utilized to evaluate the efficiency of the radiation detector. In this field, one of the major interests is on the circular shaped detector with different types of radiation sources, such as a point source [38, 39], a line source [40–43], a disk source [44, 45], and a ring source [46]. Also, the solid angle evaluation for different types of detector geometries have been studied as well, including a cylindrical detector [47], a well-shaped detector [48], and a detector with an elliptic shape [35, 49]. On the other hand, one of the important similarities between the view factor and the solid angle is that both quantities remain invariant by evaluating the perspective projection of the target geometry. Therefore, for both quantities, the transformation of the original target geometry to its perspective projection is a useful approach to simplify the calculation.

The detailed evaluation processes for the ellipse and ellipsoid view factors are presented in Section 2 and Section 3, respectively. Finally, the derived view factor expressions are evaluated for various parameters, and compared with the numerical results in Section 4.

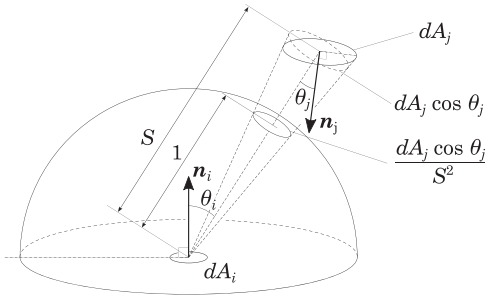

FIGURE 2 | Concept of solid angle and view factor between differential surfaces.

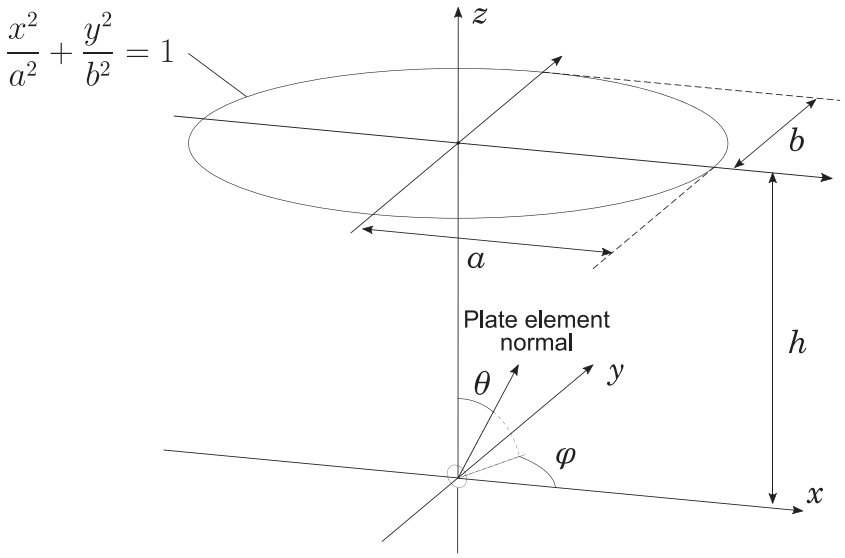

FIGURE 1 | Ellipse view factor from a plate element which is placed on the normal line passing through the ellipse center. The analytical solutions are presented in the previous study [34].

2 | View Factor of an Ellipse

In this section, the view factor of an ellipse from a plate element in an arbitrary position and orientation is evaluated. Without loss of generality, it is assumed that the plate element is placed at the origin, and the ellipse is located as shown in Equation (3), where (x_c, y_c, z_c) is the center of the ellipse, and a, b are the lengths of the ellipse semi-axes. The evaluation focuses on the ellipse surface facing towards the $-z$ direction, and z_c takes a positive value.

$$\left(\frac{x-x_c}{a}\right)^2+\left(\frac{y-y_c}{b}\right)^2=1, \text{and} \quad z=z_c. \tag{3}$$

The orientation of the plate element is described by the normal vector $\boldsymbol{n}_{\text{plate}}$ as shown in Equation (4), where the angular parameter ranges are $0 \le \theta \le \pi$ and $0 \le \varphi \le 2\pi$.

$$\boldsymbol{n}_{\text{plate}}=\begin{bmatrix} n_x \\ n_y \\ n_z \end{bmatrix}=\begin{bmatrix} \sin\theta\cos\varphi \\ \sin\theta\sin\varphi \\ \cos\theta \end{bmatrix}, \tag{4}$$

Given the complexity of the view factor calculation in this configuration, the perspective projection of the ellipse is employed to simplify the evaluation. As shown in Figure 3, the objective is to find the orientation of the image plane, such that the perpendicular line from the plate element to the image plane passes through the center of the ellipse, and the X and Y axes of the image plane are aligned with the semi-major and semi-minor axes of the image ellipse. In general, the perpendicular line from the plate element to the image plane does not pass through the center of the image ellipse [50, 51]. To find the correct orientation, the following procedure can be utilized. First, an elliptic cone, which bounds the ellipse and passes through the origin as the apex is described as a quadratic form. Next, the eigenvalue problem of the corresponding matrix is solved, to determine its eigenvalues and eigenvectors. This approach is analogous to the solid angle evaluation method presented by Conway [35] and Heitz [36, 37]. Conway introduced the idea of transforming an ellipsoid to a corresponding ellipse by using a rotation matrix, and the related rotation parameters are specified by solving the cubic polynomial in the end. Heitz replaced this procedure with an equivalent eigenvalue problem, and the solutions are calculated with the aid of the MATLAB library. In this study, the transformation is performed based on Heitz's approach because of the methodological conciseness, but the final transformation parameters are acquired in the explicit analytical form.

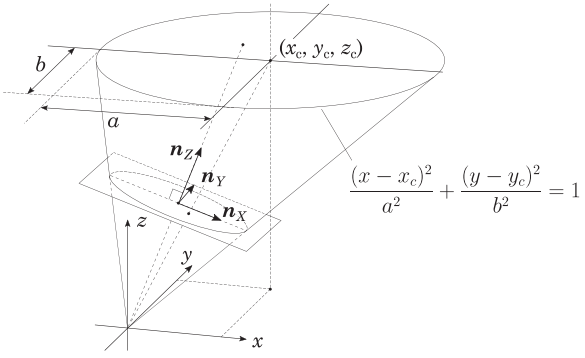

FIGURE 3 | Perspective projection of an ellipse. The perpendicular line from the plate element to the image plane passes through the center of the image ellipse.

The elliptic cone, which bounds this ellipse and the origin as the apex, is described by

$$\left(\frac{x}{a}-\frac{x_c z}{a z_c}\right)^2+\left(\frac{y}{b}-\frac{y_c z}{b z_c}\right)^2=\left(\frac{z}{z_c}\right)^2. \tag{5}$$

This equation can be rewritten in the matrix form as

$$\boldsymbol{x}^{\mathrm{T}} M \boldsymbol{x}=0, \tag{6}$$

where

$$M=\begin{bmatrix} \frac{z_c^2}{a^2} & 0 & -\frac{x_c z_c}{a^2} \\ 0 & \frac{z_c^2}{b^2} & -\frac{y_c z_c}{b^2} \\ -\frac{x_c z_c}{a^2} & -\frac{y_c z_c}{b^2} & \frac{x_c^2}{a^2}+\frac{y_c^2}{b^2}-1 \end{bmatrix}, \boldsymbol{x}=\begin{bmatrix} x \\ y \\ z \end{bmatrix}. \tag{7}$$

The characteristic polynomial of this matrix is given by

$$\chi(\lambda)=\lambda^3+A\lambda^2+B\lambda+C, \tag{8}$$

where

$$A=1-\frac{x_c^2}{a^2}-\frac{y_c^2}{b^2}-\frac{z_c^2}{a^2}-\frac{z_c^2}{b^2}, \tag{9}$$

$$B=\frac{\left(x_c^2+y_c^2+z_c^2\right)z_c^2}{a^2b^2}-\frac{z_c^2}{a^2}-\frac{z_c^2}{b^2}, \tag{10}$$

$$C=\frac{z_c^4}{a^2b^2}. \tag{11}$$

Since the matrix is regular and real-symmetric, it has three real eigenvalues, and the corresponding eigenvectors are orthogonal to each other. Considering the geometrical relation, the eigenvalues are expected to be either (positive, positive, and negative) or (negative, negative, and positive). In addition, $\chi(0) > 0$ is satisfied, which indicates that the applicable eigenvalue configuration is (positive, positive, and negative).

The eigenvalues are obtained by solving the cubic equation Equation (8). The method employed to specify the roots and the explicit expressions are presented in Appendix A. In the following discussion, the eigenvalues are denoted as λ_1, λ_2, and λ_3, where λ_2 is the smallest eigenvalue.

The eigenvalue related to the axis direction of the elliptic cone is λ_2. We align the new X-axis with the eigenvector corresponding to λ_3, and the new Y-axis with the eigenvector corresponding to

λ_1. The corresponding eigenvector for λ_2 is given by Equation (13), considering that the z-component should be positive. After normalizing the eigenvectors, the new base vectors $\boldsymbol{n}_X$, $\boldsymbol{n}_Y$, and $\boldsymbol{n}_Z$ are specified as shown in Equation (12).

$$\boldsymbol{n}_Z = \frac{\boldsymbol{n}_2}{|\boldsymbol{n}_2|}, \boldsymbol{n}_X = \frac{\boldsymbol{n}_3}{|\boldsymbol{n}_3|}, \boldsymbol{n}_Y = \boldsymbol{n}_Z \times \boldsymbol{n}_X, \tag{12}$$

$$\boldsymbol{n}_2 = \begin{bmatrix} -\frac{x_c z_c}{a^2}\left(\lambda_2 - \frac{z_c^2}{b^2}\right) \\ -\frac{y_c z_c}{b^2}\left(\lambda_2 - \frac{z_c^2}{a^2}\right) \\ \left(\lambda_2 - \frac{z_c^2}{a^2}\right)\left(\lambda_2 - \frac{z_c^2}{b^2}\right) \end{bmatrix}, \tag{13}$$

$$\boldsymbol{n}_3 = \begin{bmatrix} -\frac{x_c z_c}{a^2}\left(\lambda_3 - \frac{z_c^2}{b^2}\right) \\ -\frac{y_c z_c}{b^2}\left(\lambda_3 - \frac{z_c^2}{a^2}\right) \\ \left(\lambda_3 - \frac{z_c^2}{a^2}\right)\left(\lambda_3 - \frac{z_c^2}{b^2}\right) \end{bmatrix}. \tag{14}$$

The elliptic cone in the new coordinate system is described by Equation (15), and the plate element orientation in the new coordinate system $\boldsymbol{N}_{\text{plate}}$ is given by Equation (16).

$$\lambda_3 X^2 + \lambda_1 Y^2 = -\lambda_2 Z^2. \tag{15}$$

$$\boldsymbol{N}_{\text{plate}} = [\boldsymbol{n}_X \quad \boldsymbol{n}_Y \quad \boldsymbol{n}_Z]^{\mathrm{T}} \boldsymbol{n}_{\text{plate}}, \tag{16}$$

where the angular parameters Θ and Φ in the new coordinate system are related as shown in Equation (17).

$$\boldsymbol{N}_{\text{plate}} = \begin{bmatrix} \sin\Theta\cos\Phi \\ \sin\Theta\sin\Phi \\ \cos\Theta \end{bmatrix}. \tag{17}$$

Using this transformation, the original ellipse view factor is calculated as a view factor shown in Figure 4, where the analytical solution is available in the previous study [34]. The view factor solution for Figure 4 configuration is classified into three cases, depending on whether the extended surface of the plate element has an intersection with the ellipse. When the conditions of Equations (18) and (19) are satisfied, the plate element surface does not intersect the ellipse, and the entire ellipse is visible from the plate element.

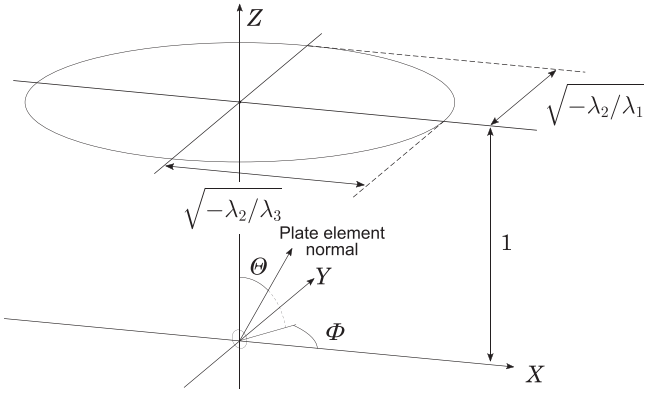

FIGURE 4 | Projected ellipse on the image plane which subtends the same view factor as the original ellipse.

$$b^2 n_y^2 + a^2 n_x^2 < (n_x x_c + n_z z_c + n_y y_c)^2, \tag{18}$$

$$n_x x_c + n_z z_c + n_y y_c > 0. \tag{19}$$

In this case, the view factor from the plate element to the ellipse is expressed by Equation (20).

$$F_{\text{ellipse}} = \frac{-\lambda_2 \cos\Theta}{\sqrt{(-\lambda_2 + \lambda_3)(-\lambda_2 + \lambda_1)}}. \tag{20}$$

On the other hand, if the conditions of Equations (18) and (21) are satisfied, the ellipse is not visible from the plate element.

$$n_x x_c + n_z z_c + n_y y_c < 0. \tag{21}$$

Therefore, the corresponding ellipse view factor is presented as Equation (22).

$$F_{\text{ellipse}} = 0. \tag{22}$$

3 | View Factor of an Ellipsoid

The view factor of an ellipsoid from a plate element is evaluated by the same approach as the ellipse view factor. The ellipsoid is described by Equation (23), where (x_c, y_c, z_c) is the center of the ellipsoid, and a, b, c are the lengths of the ellipsoid semi-axes. The plate element is assumed to be located at the origin, and its orientation $\boldsymbol{n}_{\text{plate}}$ is described by Equation (4). Additionally, it should be noted that the origin lies outside the ellipsoid, and z_c value can take a negative value as well.

$$\frac{(x - x_c)^2}{a^2} + \frac{(y - y_c)^2}{b^2} + \frac{(z - z_c)^2}{c^2} = 1. \tag{23}$$

As shown in Figure 5, the correct orientation of the image plane should be specified, such that the perpendicular line from the plate element to the image plane passes through the center of the image ellipse, and the X and Y axes of the image plane are aligned with the semi-major and semi-minor axes of the image ellipse.

The perspective projection of an ellipsoid is commonly utilized in the field of computer graphics and computer vision. For the applications in augmented reality (AR) or robotics, camera pose estimation from 2D images is a fundamental task. One approach for such task is to abstract the 3D objects as ellipsoids and estimate the pose of the camera from the projected ellipses [52]. Also, in the field of spacecraft navigation, the perspective projection of ellipses and ellipsoids is employed for the recognition of a planetary body [53] or craters on the surface [54]. The basic methodology utilized in these research works is

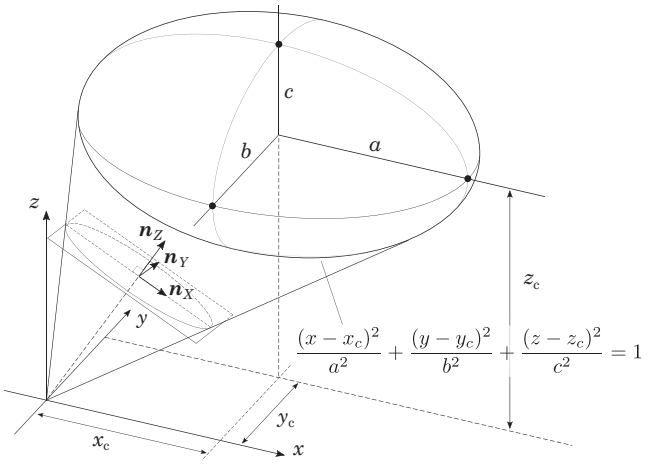

FIGURE 5 | Perspective projection of an ellipsoid. The perpendicular line from the plate element to the image plane passes through the center of the image ellipse.

presented by Eberly [55] and this methodology is utilized in this study as well. According to this report, the elliptic cone, which tightly bounds the ellipsoid, is described by

$$\boldsymbol{x}^{\mathrm{T}}\Big(D\boldsymbol{x}_c\boldsymbol{x}_c^{\mathrm{T}}D-\Big(\boldsymbol{x}_c^{\mathrm{T}}D\boldsymbol{x}_c-1\Big)D\Big)\boldsymbol{x}=0, \tag{24}$$

where

$$D=\begin{bmatrix}\frac{1}{a^2}&0&0\\0&\frac{1}{b^2}&0\\0&0&\frac{1}{c^2}\end{bmatrix},\boldsymbol{x}_c=\begin{bmatrix}x_c\\y_c\\z_c\end{bmatrix}. \tag{25}$$

The matrix in Equation (24) is explicitly expressed by

$$\begin{aligned}&D\boldsymbol{x}_c\boldsymbol{x}_c^{\mathrm{T}}D-\Big(\boldsymbol{x}_c^{\mathrm{T}}D\boldsymbol{x}_c-1\Big)D\\&=\begin{bmatrix}\frac{1}{a^2}-\frac{y_c^2}{a^2b^2}-\frac{z_c^2}{a^2c^2}&\frac{x_cy_c}{a^2b^2}&\frac{x_cz_c}{a^2c^2}\\\frac{x_cy_c}{a^2b^2}&\frac{1}{b^2}-\frac{x_c^2}{a^2b^2}-\frac{z_c^2}{b^2c^2}&\frac{y_cz_c}{b^2c^2}\\\frac{x_cz_c}{a^2c^2}&\frac{y_cz_c}{b^2c^2}&\frac{1}{c^2}-\frac{x_c^2}{a^2c^2}-\frac{y_c^2}{b^2c^2}\end{bmatrix}.\end{aligned} \tag{26}$$

The characteristic polynomial of the matrix is described by

$$\chi(\lambda)=\lambda^3+A\lambda^2+B\lambda+C, \tag{27}$$

where

$$A=\frac{x_c^2+y_c^2}{a^2b^2}+\frac{y_c^2+z_c^2}{b^2c^2}+\frac{x_c^2+z_c^2}{a^2c^2}-\frac{1}{a^2}-\frac{1}{b^2}-\frac{1}{c^2}, \tag{28}$$

$$B=\frac{x_c^2+y_c^2+z_c^2-a^2-b^2-c^2}{a^2b^2c^2}\left(\frac{x_c^2}{a^2}+\frac{y_c^2}{b^2}+\frac{z_c^2}{c^2}-1\right), \tag{29}$$

$$C=-\frac{\left(-a^2b^2c^2+a^2b^2z_c^2+a^2c^2y_c^2+b^2c^2x_c^2\right)^2}{a^6b^6c^6}. \tag{30}$$

The matrix shown in Equation (26) is regular and real-symmetric. Thus, the characteristic polynomial has three real eigenvalues, and the corresponding eigenvectors are orthogonal to each other. Since $\chi(0)<0$, it should have roots of (positive, positive, and positive) or (negative, negative, and positive). Considering the expected geometry after diagonalization, the applicable configuration is two negative roots and one positive root. These roots, denoted as λ_1,λ_2, and λ_3, are determined as described in Appendix A. The largest eigenvalue λ_1 is related to the perpendicular line direction from the plate element to the image plane. The corresponding eigenvectors are specified by Equations (31) and (32). Since two opposite directions are possible for the perpendicular vector with respect to the image plane, we select the direction towards the ellipsoid as $\boldsymbol{n}_Z$ as shown in Equation (31). Then, the remaining base vectors $\boldsymbol{n}_X$ and $\boldsymbol{n}_Y$ are determined as shown in Equation (32).

$$\boldsymbol{n}_Z=\begin{cases}+\dfrac{\boldsymbol{n}_1}{|\boldsymbol{n}_1|}, & \text{if } \boldsymbol{n}_1\cdot\boldsymbol{x}_c>0\\-\dfrac{\boldsymbol{n}_1}{|\boldsymbol{n}_1|}, & \text{otherwise}\end{cases}, \tag{31}$$

$$\boldsymbol{n}_X=\frac{\boldsymbol{n}_3}{|\boldsymbol{n}_3|},\boldsymbol{n}_Y=\boldsymbol{n}_Z\times\boldsymbol{n}_X, \tag{32}$$

where

$$\boldsymbol{n}_1=\begin{bmatrix}\frac{x_cy_c^2z_c}{a^2b^4c^2}+\frac{x_cz_c}{a^2c}\left(\lambda_1+\frac{x_c^2}{a^2b^2}+\frac{z_c^2}{b^2c^2}-\frac{1}{b^2}\right)\\\frac{x_c^2y_cz_c}{a^4b^2c^2}+\frac{y_cz_c}{b^2c^2}\left(\lambda_1+\frac{y_c^2}{a^2b^2}+\frac{z_c^2}{a^2c^2}-\frac{1}{a^2}\right)\\\left(\lambda_1+\frac{y_c^2}{a^2b^2}+\frac{z_c^2}{a^2c^2}-\frac{1}{a^2}\right)\\\left(\lambda_1+\frac{x_c^2}{a^2b^2}+\frac{z_c^2}{b^2c^2}-\frac{1}{b^2}\right)-\frac{x_c^2y_c^2}{a^4b^4}\end{bmatrix}, \tag{33}$$

$$\boldsymbol{n}_3=\begin{bmatrix}\frac{x_cy_c^2z_c}{a^2b^4c^2}+\frac{x_cz_c}{a^2c^2}\left(\lambda_3+\frac{x_c^2}{a^2b^2}+\frac{z_c^2}{b^2c^2}-\frac{1}{b^2}\right)\\\frac{x_c^2y_cz_c}{a^4b^2c^2}+\frac{y_cz_c}{b^2c^2}\left(\lambda_3+\frac{y_c^2}{a^2b^2}+\frac{z_c^2}{a^2c^2}-\frac{1}{a^2}\right)\\\left(\lambda_3+\frac{y_c^2}{a^2b^2}+\frac{z_c^2}{a^2c^2}-\frac{1}{a^2}\right)\left(\lambda_3+\frac{x_c^2}{a^2b^2}\right.\\\left.+\frac{z_c^2}{b^2c^2}-\frac{1}{b^2}\right)-\frac{x_c^2y_c^2}{a^4b^4}\end{bmatrix}. \tag{34}$$

If the obtained $\boldsymbol{n}_1$ or $\boldsymbol{n}_3$ is a zero vector, the following formula can be used alternatively.

$$\boldsymbol{n}_1 = \begin{bmatrix} -\dfrac{x_c y_c z_c^2}{a^2b^2c^4} - \dfrac{x_c y_c}{a^2b^2}\left(\lambda_1 + \dfrac{x_c^2}{a^2c^2} + \dfrac{y_c^2}{b^2c^2} - \dfrac{1}{c^2}\right) \\ \dfrac{x_c^2 z_c^2}{a^4c^4} - \left(\lambda_1 + \dfrac{x_c^2}{a^2c^2} + \dfrac{y_c^2}{b^2c^2} - \dfrac{1}{c^2}\right) \\ \left(\lambda_1 + \dfrac{y_c^2}{a^2b^2} + \dfrac{z_c^2}{a^2c^2} - \dfrac{1}{a^2}\right) \\ -\dfrac{x_c^2 y_c z_c}{a^4b^2c^2} + \dfrac{y_c z_c}{b^2c^2}\left(\lambda_1 + \dfrac{y_c^2}{a^2b^2} + \dfrac{z_c^2}{a^2c^2} - \dfrac{1}{a^2}\right) \end{bmatrix}, \quad (35)$$

$$\boldsymbol{n}_3 = \begin{bmatrix} -\dfrac{x_c y_c z_c^2}{a^2b^2c^4} - \dfrac{x_c y_c}{a^2b^2}\left(\lambda_3 + \dfrac{x_c^2}{a^2c^2} + \dfrac{y_c^2}{b^2c^2} - \dfrac{1}{c^2}\right) \\ \dfrac{x_c^2 z_c^2}{a^4c^4} - \left(\lambda_3 + \dfrac{x_c^2}{a^2c^2} + \dfrac{y_c^2}{b^2c^2} - \dfrac{1}{c^2}\right) \\ \left(\lambda_3 + \dfrac{y_c^2}{a^2b^2} + \dfrac{z_c^2}{a^2c^2} - \dfrac{1}{a^2}\right) \\ -\dfrac{x_c^2 y_c z_c}{a^4b^2c^2} + \dfrac{y_c z_c}{b^2c^2}\left(\lambda_3 + \dfrac{y_c^2}{a^2b^2} + \dfrac{z_c^2}{a^2c^2} - \dfrac{1}{a^2}\right) \end{bmatrix}. \quad (36)$$

The elliptic cone in the new coordinate system is described by Equation (37), and the plate element orientation in the new coordinate system is given by Equations (16)–(17) same as in the ellipse case. Based on this transformation, the original ellipsoid view factor can be calculated as the ellipse view factor shown in Figure 6.

$$-\lambda_3 X^2 - \lambda_2 Y^2 = \lambda_1 Z^2. \quad (37)$$

If the conditions in Equations (38) and (19) are satisfied, the plate element surface does not intersect the ellipsoid, and the entire ellipsoid is visible from the plate element.

$$a^2 n_x^2 + b^2 n_y^2 + c^2 n_z^2 < (n_x x_c + n_y y_c + n_z z_c)^2. \quad (38)$$

In this case, the view factor from the plate element to the ellipsoid is expressed as

$$F_{\text{ellipsoid}} = \frac{\lambda_1 \cos\Theta}{\sqrt{(-\lambda_1 + \lambda_3)(-\lambda_1 + \lambda_2)}}. \quad (39)$$

On the other hand, if the conditions of Equations (38) and (21) are satisfied, the ellipsoid is not visible from the plate element. Therefore, the corresponding ellipsoid view factor is presented as

$$F_{\text{ellipsoid}} = 0. \quad (40)$$

4 | Numerical Validation

4.1 | Ellipse View Factor Validation

The numerical calculation of an ellipse view factor can be performed by integrating view factors of individual mesh elements. In this test, $2a \times 2b$ rectangular area is divided into 4000×4000 mesh elements, as shown in Figure 7. A view factor for single mesh element is calculated based on Equation (2) with the parameters shown in Equations (41)–(44). For each element, a central position of the mesh element is checked if it lies inside the ellipse, and element view factors within the ellipse are summed to evaluate the ellipse view factor.

$$S^2 = x^2 + y^2 + z_c^2, \quad (41)$$

$$\cos\theta_i = \frac{1}{S}\begin{bmatrix} x \\ y \\ z_c \end{bmatrix} \cdot \begin{bmatrix} \sin\theta\cos\varphi \\ \sin\theta\sin\varphi \\ \cos\theta \end{bmatrix}, \quad (42)$$

$$\cos\theta_j = -\frac{1}{S}\begin{bmatrix} x \\ y \\ z_c \end{bmatrix} \cdot \begin{bmatrix} 0 \\ 0 \\ -1 \end{bmatrix}, \quad (43)$$

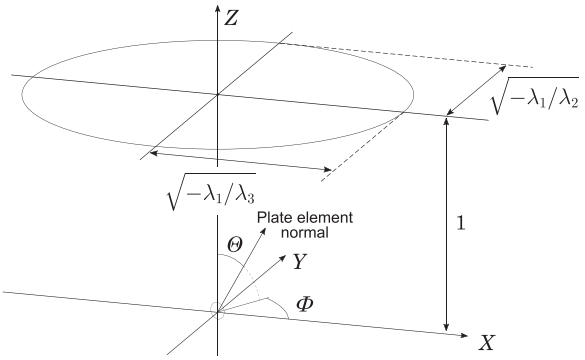

FIGURE 6 | Projected ellipse on the image plane which subtends the same view factor as the original ellipsoid.

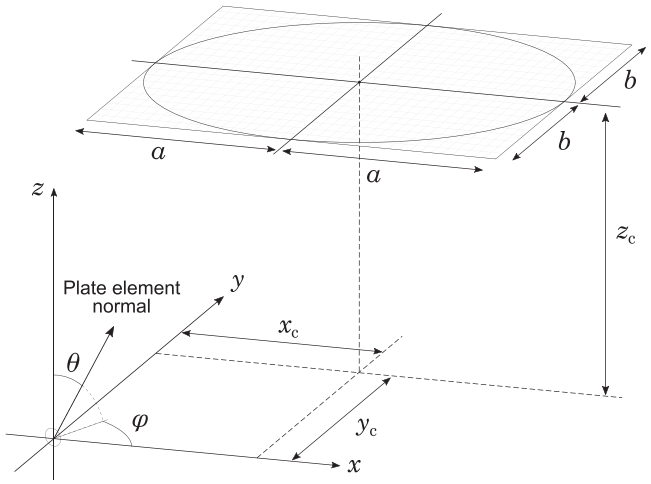

FIGURE 7 | Numerical evaluation of the ellipse view factor from a plate element.

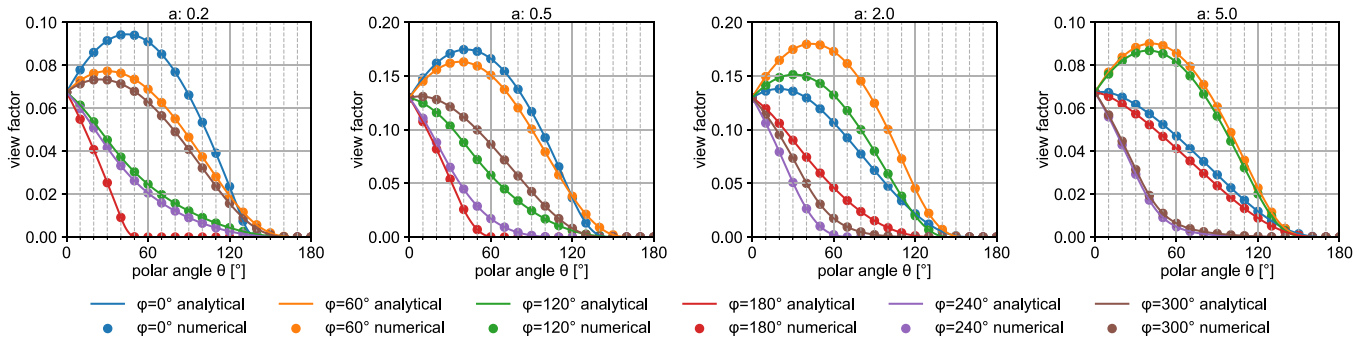

FIGURE 8 | Selected calculation results from the ellipse view factor verification cases, where the center of the ellipse is at (1, 1, 1).

TABLE 1 | Test parameters for ellipse view factor calculation.

Parameter	Values
x_c	−2.0, −1.0, −0.5, 0.5, 1.0, 2.0
y_c	−2.0, −1.0, −0.5, 0.5, 1.0, 2.0
z_c	0.5, 1.0, 2.0
a	0.2, 0.5, 2.0, 5.0
θ [°]	0, 10, 20, ··· 180
φ [°]	0, 30, 60, ··· 330

Note: The parameter b is specified by $ab = 1$. The total number of test cases is 98,496.

$$dA_j = dxdy. \tag{44}$$

The parameters used for the validation tests are summarized in Table 1. For all test cases, the differences between the numerical and analytical results are within 1.0×10^{-6}. Additionally, selected test results, with the ellipse center at (1, 1, 1), are presented in Figure 8.

4.2 | Ellipsoid View Factor Validation

The numerical calculation of the ellipsoid view factor can be performed by integrating the view factor of mesh elements over the ellipsoid surface. The ellipsoid surface for Equation (23) is presented by the parametric form as

$$\begin{bmatrix} x \\ y \\ z \end{bmatrix} = \begin{bmatrix} x_c \\ y_c \\ z_c \end{bmatrix} + \begin{bmatrix} a \sin\alpha \cos\beta \\ b \sin\alpha \sin\beta \\ c \cos\alpha \end{bmatrix}, \tag{45}$$

where α is the polar angle and β is the azimuthal angle as shown in Figure 9. The mesh elements are generated by dividing the ellipsoid surface into 4000×4000 sections along the α and β directions. The partial derivatives of Equation (23) with respect to α and β are the tangential vectors of the ellipsoid surface. The differential surface area dA_j and the normal vector $\boldsymbol{n}_j$ are determined by evaluating the vector product of these tangential vectors.

$$dA_j = \sqrt{c^2(b^2\cos^2\beta + a^2\sin^2\beta)\sin^2\alpha + a^2b^2\cos^2\alpha} \times \sin\alpha d\alpha d\beta, \tag{46}$$

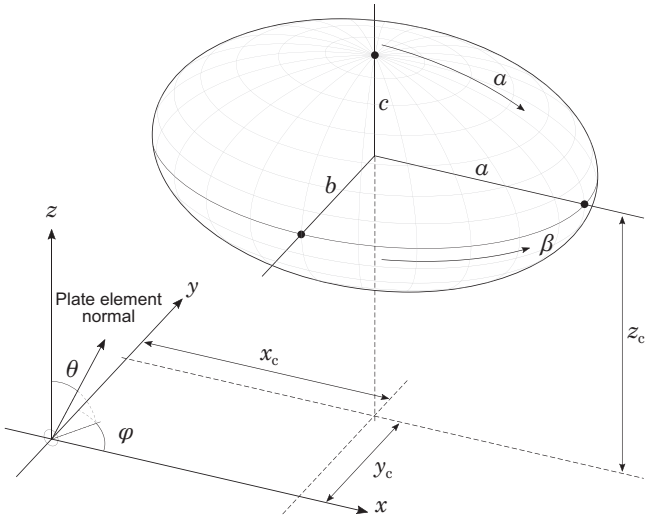

FIGURE 9 | Numerical evaluation of the ellipsoid view factor from a plate element.

$$\boldsymbol{n}_j = \frac{1}{\sqrt{c^2(b^2\cos^2\beta + a^2\sin^2\beta)\sin^2\alpha + a^2b^2\cos^2\alpha}} \times \begin{bmatrix} bc\sin\alpha\cos\beta \\ ac\sin\alpha\sin\beta \\ ab\cos\alpha \end{bmatrix}. \tag{47}$$

The view factor of each mesh element is calculated by Equation (2), and related variables are calculated by

$$S^2 = x^2 + y^2 + z^2, \tag{48}$$

$$\cos\theta_i = \frac{1}{S}\begin{bmatrix} x \\ y \\ z \end{bmatrix} \cdot \begin{bmatrix} \cos\theta\cos\varphi \\ \cos\theta\sin\varphi \\ \sin\theta \end{bmatrix}, \tag{49}$$

$$\cos\theta_j = -\frac{1}{S\sqrt{c^2(b^2\cos^2\beta + a^2\sin^2\beta)\sin^2\alpha + a^2b^2\cos^2\alpha}} \times \begin{bmatrix} x \\ y \\ z \end{bmatrix} \cdot \begin{bmatrix} bc\sin\alpha\cos\beta \\ ac\sin\alpha\sin\beta \\ ab\cos\alpha \end{bmatrix}. \tag{50}$$

TABLE 2 | Test parameters for ellipsoid view factor calculation.

Parameter	Values
x_c	−1.0, 0.5, 1.0, 2.0
y_c	−1.0, 0.5, 1.0, 2.0
z_c	−1.0, 0.5, 1.0, 2.0
a	0.2, 0.5, 2.0, 5.0
b	0.2, 0.5, 2.0, 5.0
θ [°]	0, 10, 20, ··· 180
φ [°]	0, 30, 60, ··· 330

Note: The parameter c is specified by $abc = 1$. The total number of test cases is 233,472.

The parameters used in the validation tests are summarized in Table 2. With respect to the amount of error between the numerical and analytical results, 99.46% of the test cases show errors within 1.0×10^{-6}, 0.53% of the test cases present errors between 1.0×10^{-6} and 1.0×10^{-5}, and the other 0.01% of the test cases exhibit errors greater than 1.0×10^{-5}. The error values greater than 1.0×10^{-5} are found in 24 cases with the parameter set of $a = 0.2, b = 0.2, x_c = 0.5, y_c = 0.5, z_c = 0.5$. An error in each numerical result is caused by the midpoint method and the inaccuracy of the integration area represented by the mesh. With these two effects, the amount of error is not necessarily monotonously decreasing, while increasing the number of mesh elements. However, it is expected that the amount of error tends to decrease by increasing the number of

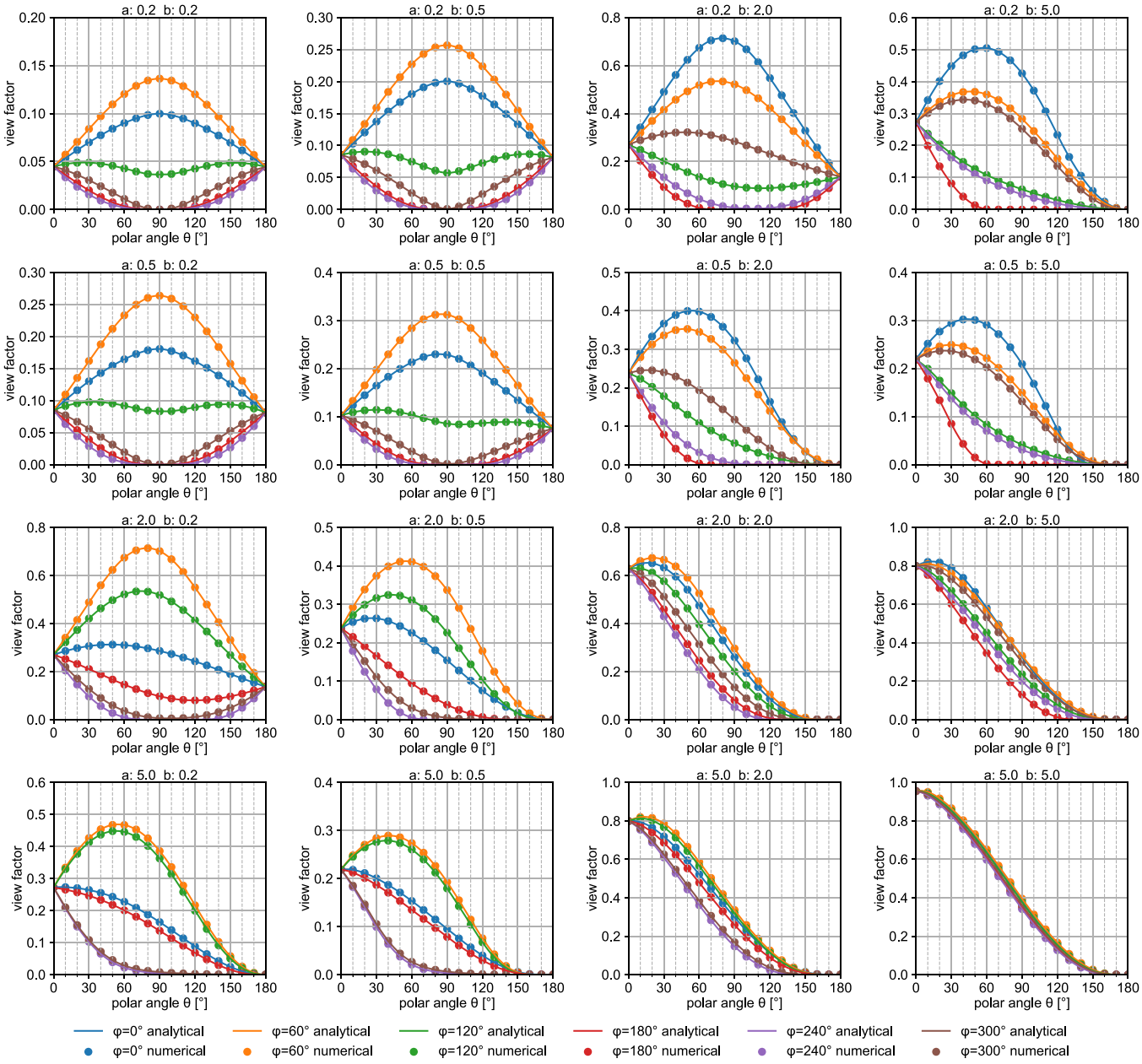

FIGURE 10 | Selected calculation results from the ellipsoid view factor verification cases, where the center of the ellipsoid is at (1, 1, 1).

mesh elements, until the effect of integrated floating point error becomes significant. Indeed, the observed maximum error in $a = 0.2, b = 0.2, x_c = 0.5, y_c = 0.5, z_c = 0.5$ cases is 1.64×10^{-5} for 4000×4000 mesh, and it can be reduced to 5.47×10^{-7} for 10000×10000 mesh. From these results, there is no indication of incorrectness in the analytical results, and the error between analytical and numerical results can be reduced by finer mesh for numerical integration. Additionally, selected test results, with the ellipse center at (1, 1, 1), are presented in Figure 10.

5 | Conclusion

This study analytically derived the view factors of an ellipse and an ellipsoid from a plate element for arbitrary positions and orientations. These results are generalizations of the view factors of a sphere and a circle, the solutions of which were precisely investigated in previous studies. The sphere and circle view factors are used in various fields, such as the thermal radiation analysis of a fireball, the lighting evaluation, and the heat flux analysis of an earth-orbiting spacecraft. The extension of the analytical view factor calculation to an ellipse and an ellipsoid is expected to be useful for further applications, such as thermal radiation analysis of jet fires, plant canopies, aerostats, or celestial bodies.

Despite their potential applications, the extension to the elliptical geometries presented significant challenges. Compared to the sphere and circle cases, the ellipse and ellipsoid view factors involve more mathematical complexity, and the general analytical solutions had not been established. In this study, we demonstrated that the perspective projection approach enables the derivation of explicit analytical solutions for ellipse and ellipsoid view factors. By analyzing the projections of the ellipse and ellipsoid, the original view factor calculation has been transformed into an equivalent ellipse view factor problem with known analytical solutions. This transformation methodology is analogous to solid angle evaluation techniques for an ellipse and an ellipsoid, and the methodology has been extended specifically for view factor calculations with explicit analytical expressions.

The extensive numerical tests with various geometrical parameters have been performed to confirm the validity of the derived expressions. In the numerical calculations, the view factors of an ellipse and an ellipsoid were evaluated by integrating the view factors of individual mesh elements. The test results presented that the differences between analytical and numerical results are within 1.0×10^{-6} for the all ellipse cases and for most ellipsoid cases. Some test cases with slightly larger errors were additionally evaluated with finer numerical integration meshes. The results showed the errors were reduced below 1.0×10^{-6}, which further validated our analytical approach.

Nomenclature

Roman symbols

a, b, c	length of semi-axes of an ellipse or an ellipsoid
A, B, C	coefficients of the characteristic polynomial
D	matrix describing the ellipsoid
dA_i	differential area of the plate element on the source side
dA_j	differential area of the plate element on the target side
dF	differential view factor
F_{ellipse}	view factor of an ellipse from a plate element
$F_{\text{ellipsoid}}$	view factor of an ellipsoid from a plate element
h	distance between the plate element and the ellipse
M	matrix describing the elliptic cone for ellipse view factor evaluation
$\boldsymbol{n}_1, \boldsymbol{n}_2, \boldsymbol{n}_3$	eigenvectors of the elliptic cone matrix
$\boldsymbol{n}_i$	normal vector of the plate element on the source side
$\boldsymbol{n}_j$	normal vector of the plate element on the target side
$\boldsymbol{n}_{\text{plate}}$	normal vector of the plate element in the original coordinate system
$\boldsymbol{N}_{\text{plate}}$	normal vector of the plate element in the transformed coordinate system
$\boldsymbol{n}_X, \boldsymbol{n}_Y, \boldsymbol{n}_Z$	base vectors of the transformed coordinate system
p, q	coefficients of the reduced cubic equation
S	distance between the plate element and the target surface
x, y, z	Cartesian coordinates
x_c, y_c, z_c	coordinates of the center of the ellipse or ellipsoid
X, Y, Z	transformed Cartesian coordinates

Greek symbols

α, β	parametric angles for ellipsoid surface used for numerical calculation
$\lambda_1, \lambda_2, \lambda_3$	eigenvalues of the elliptic cone matrix
$\Lambda_1, \Lambda_2, \Lambda_3$	shifted eigenvalues in cubic equation analysis
θ	polar angle of the plate element normal in the original coordinate system
θ_i	angle between the source plate element normal and the line connecting the source and target plate elements
θ_j	angle between the target plate element normal and the line connecting the source and target plate elements
Θ	polar angle of the plate element normal in the transformed coordinate system
φ	azimuthal angle of the plate element normal in the original coordinate system
Φ	azimuthal angle of the plate element normal in the transformed coordinate system
$\chi(\lambda)$	characteristic polynomial
$d\Omega$	differential solid angle

Acknowledgments

Open Access funding enabled and organized by Projekt DEAL.

Conflicts of Interest

The author declares no conflicts of interest.

Data Availability Statement

The data that support the findings of this study are available from the corresponding author upon reasonable request.

References

1. A. Narayanaswamy, "An Analytic Expression for Radiation View Factor Between Two Arbitrarily Oriented Planar Polygons," *International Journal of Heat and Mass Transfer* 91 (2015): 841–847, https://doi.org/10.1016/j.ijheatmasstransfer.2015.07.131.

2. H. Zhao and Y. Zhang, "Method of Spherical Triangle-Division for Solving View Factors in Built Environment and Its Application for Non-Uniform Thermal Radiation Environments," *Building and Environment* 222 (2022): 109360, https://doi.org/10.1016/j.buildenv.2022.109360.

3. Y. Camaraza-Medina, A. Hernandez-Guerrero, and J. L. Luviano-Ortiz, "Analytical View Factor Solution for Radiant Heat Transfer Between Two Arbitrary Rectangular Surfaces," *Journal of Thermal Analysis and Calorimetry* 147 (2022): 14999–15016, https://doi.org/10.1007/s10973-022-11646-4.

4. J. R. Howell and M. P. Mengüç, "Radiative Transfer Configuration Factor Catalog: A Listing of Relations for Common Geometries," *Journal of Quantitative Spectroscopy and Radiative Transfer* 112, no. 5 (2011): 910–912, https://doi.org/10.1016/j.jqsrt.2010.10.002.

5. J. R. Howell, "A Catalogue of Radiation Heat Transfer Configuration Factors," Online resource; 2020.

6. J. Vílchez, M. Muñoz, J. Bonilla, and E. Planas, "Configuration Factors for Ground Level Fireballs With Shadowing," *Journal of Loss Prevention in the Process Industries* 51 (2018): 169–177, https://doi.org/10.1016/j.jlp.2017.12.010.

7. J. Bonilla, A. Águeda, M. Muñoz, J. Vílchez, and E. Planas, "Thermal Radiation Model for Dynamic Fireballs With Shadowing," *Process Safety and Environmental Protection* 128 (2019): 372–384, https://doi.org/10.1016/j.psep.2019.05.029.

8. A. Peña-García and J. Cabeza-Lainez, "Daylighting of Road Tunnels Through External Ground-Based Light-Pipes and Complex Reflective Geometry," *Tunnelling and Underground Space Technology* 131 (2023): 104788, https://doi.org/10.1016/j.tust.2022.104788.

9. J. Cabeza-Lainez, "A New Principle for Building Simulation of Radiative Heat Transfer in the Presence of Spherical Surfaces," *Buildings* 13, no. 6 (2023): 1447, https://doi.org/10.3390/buildings13061447.

10. J. Li, S. Yan, and R. Cai, "Thermal Analysis of Composite Solar Array Subjected to Space Heat Flux," *Aerospace Science and Technology* 27, no. 1 (2013): 84–94, https://doi.org/10.1016/j.ast.2012.06.010.

11. M. Bulut and N. Sozbir, "Analytical Investigation of a Nanosatellite Panel Surface Temperatures for Different Altitudes and Panel Combinations," *Applied Thermal Engineering* 75 (2015): 1076–1083, https://doi.org/10.1016/j.applthermaleng.2014.10.059.

12. M. H. N. Naraghi and B. T. F. Chung, "Radiation Configuration Factors Between Disks and a Class of Axisymmetric Bodies," *Journal of Heat Transfer* 104, no. 3 (1982): 426–431, https://doi.org/10.1115/1.3245110.

13. J. M. Cabeza-Lainez, J. A. Pulido-Arcas, and M. V. Castilla, "New Configuration Factor Between a Circle, a Sphere and a Differential Area At Random Positions," *Journal of Quantitative Spectroscopy and Radiative Transfer* 129 (2013): 272–276, https://doi.org/10.1016/j.jqsrt.2013.06.027.

14. J. M. Cabeza-Lainez, J. A. Pulido-Arcas, B. Sanchez-Montañés, and C. Rubio-Bellido, "New Configuration Factor Between a Circle and a Point-Plane at Random Positions," *International Journal of Heat and Mass Transfer* 69 (2014): 147–150, https://doi.org/10.1016/j.ijheatmasstransfer.2013.09.048.

15. J. Cabeza-Lainez, "New Geometric Theorems Derived From Integral Equations Applied to Radiative Transfer in Spherical Sectors and Circular Segments," *Mathematics* 12, no. 18 (2024): 2875, https://doi.org/10.3390/math12182875.

16. B. T. F. Chung and M. H. N. Naraghi, "Some Exact Solutions for Radiation View Factors From Spheres," *AIAA Journal* 19, no. 8 (1981): 1077–1081, https://doi.org/10.2514/3.7843.

17. B. T. F. Chung and M. H. N. Naraghi, "A Simpler Formulation for Radiative View Factors From Spheres to a Class of Axisymmetric Bodies," *Journal of Heat Transfer* 104, no. 1 (1982): 201–204, https://doi.org/10.1115/1.3245054.

18. M. Sabet and B. T. F. Chung, "Radiation View Factors From a Sphere to Nonintersecting Planar Surfaces," *Journal of Thermophysics and Heat Transfer* 2, no. 3 (1988): 286–288, https://doi.org/10.2514/3.56225.

19. M. H. N. Naraghi, "Radiation View Factors From Differential Plane Sources to Disks - A General Formulation," *Journal of Thermophysics and Heat Transfer* 2, no. 3 (1988): 271–274, https://doi.org/10.2514/3.96.

20. K. Sasaki and M. Sznajder, "Analytical View Factor Solutions of a Spherical Cap From an Infinitesimal Surface," *International Journal of Heat and Mass Transfer* 163 (2020): 120477, https://doi.org/10.1016/j.ijheatmasstransfer.2020.120477.

21. G. Hankinson and B. J. Lowesmith, "A Consideration of Methods of Determining the Radiative Characteristics of Jet Fires," *Combustion and Flame* 159, no. 3 (2012): 1165–1177, https://doi.org/10.1016/j.combustflame.2011.09.004.

22. M. R. Manco, M. A. Vaz, J. C. R. Cyrino, and A. Landesmann, "Ellipsoidal Solid Flame Model for Structures Under Localized Fire," *Fire Technology* 54 (2018): 1505–1532, https://doi.org/10.1007/s10694-018-0750-y.

23. M. Liu, Y. Wang, L. Luo, et al., "Segmented Line Heat Source Model for Thermal Radiation Calculation of Jet Fires in Chemical Plants," *ASME Journal of Heat and Mass Transfer* 145, no. 9 (2023): 092801, https://doi.org/10.1115/1.4062782.

24. P. D. Colaizzi, S. R. Evett, T. A. Howell, F. Li, W. P. Kustas, and M. C. Anderson, "Radiation Model for Row Crops: I. Geometric View Factors and Parameter Optimization," *Agronomy Journal* 104, no. 2 (2012): 225–240, https://doi.org/10.2134/agronj2011.0082.

25. P. D. Colaizzi, R. C. Schwartz, S. R. Evett, T. A. Howell, P. H. Gowda, and J. A. Tolk, "Radiation Model for Row Crops: II. Model Evaluation," *Agronomy Journal* 104, no. 2 (2012): 241–255, https://doi.org/10.2134/agronj2011.0083.

26. C. Parry, H. Nieto, P. Guillevic, et al., "An Intercomparison of Radiation Partitioning Models in Vineyard Canopies," *Irrigation science* 37 (2019): 239–252.

27. K. Zhang, T. Zhang, C. Spence, and F. Qi, "A New Method for Calculating the View Factor From a Wall to a Spheroidal Canopy," *Building and Environment* 241 (2023): 110419, https://doi.org/10.1016/j.buildenv.2023.110419.

28. T. Lu, X. Lin, and W. Lan, " On the Calculation Method of the View Factor for Earth to Aerostats," in 2016 35th Chinese Control Conference (CCC) (2016), 2011–2015.

29. N. Hongpeng, L. Xianwu, L. Zhibin, and L. Weiyao, " A 3-Parameter Thermal Model for the Skin of Stratospheric Airships and its Computing Analysis," in 2017 36th Chinese Control Conference (CCC) (2017), 2082–2087.

30. M. I. Alam, A. A. Pasha, A. G. A. Jameel, and U. Ahmed, "High Altitude Airship: A Review of Thermal Analyses and Design Approaches," *Archives of Computational Methods in Engineering* 30, no. 3 (2023): 2289–2339.

31. I. Pelivan, L. Drube, E. Kührt, et al., "Thermophysical Modeling of Didymos' Moon for the Asteroid Impact Mission," *Advances in Space Research* 59, no. 7 (2017): 1936–1949, https://doi.org/10.1016/j.asr.2016.12.041.

32. H. Wong, *Heat Transfer for Engineers* (Longman Group Limited, 1977).

33. R. Siegel and J. R. Howell, Thermal Radiation Heat Transfer, 3rd ed. (Hemisphere Publishing Corporation, 1992).

34. K. Sasaki, "View Factor of a Spheroid and an Ellipse From a Plate Element," *Journal of Quantitative Spectroscopy and Radiative Transfer* 326 (2024): 109102, https://doi.org/10.1016/j.jqsrt.2024.109102.

35. J. T. Conway, "Analytical Solution for the Solid Angle Subtended at Any Point by an Ellipse via a Point Source Radiation Vector Potential," *Nuclear Instruments and Methods in Physics Research Section A: Accelerators, Spectrometers, Detectors and Associated Equipment* 614, no. 1 (2010): 17–27, https://doi.org/10.1016/j.nima.2009.11.075.

36. E. Heitz, "Computing A Front-Facing Ellipse that Subtends the Same Solid Angle as an Arbitrarily Oriented Ellipse," Working Paper or Preprint; 2017.

37. E. Heitz, "Analytical Calculation of the Solid Angle Subtended by an Arbitrarily Positioned Ellipsoid to a Point Source," *Nuclear Instruments and Methods in Physics Research Section A: Accelerators, Spectrometers, Detectors and Associated Equipment* 852 (2017): 10–14, https://doi.org/10.1016/j.nima.2017.02.004.

38. F. Paxton, "Solid Angle Calculation for a Circular Disk," *Review of Scientific Instruments* 30, no. 4 (1959): 254–258, https://doi.org/10.1063/1.1716590.

39. R. Gardner and K. Verghese, "on the Solid Angle Subtended by a Circular Disc," *Nuclear Instruments and Methods* 93, no. 1 (1971): 163–167, https://doi.org/10.1016/0029-554X(71)90155-8.

40. E. Galiano and C. Pagnutti, "An Analytical Solution for the Solid Angle Subtended by a Circular Detector for a Symmetrically Positioned Linear Source," *Applied Radiation and Isotopes* 64, no. 5 (2006): 603–607, https://doi.org/10.1016/j.apradiso.2005.12.006.

41. S. Pommé, "The Solid Angle Subtended by a Circular Detector for a Linear Source," *Applied Radiation and Isotopes* 65, no. 6 (2007): 724–727, https://doi.org/10.1016/j.apradiso.2006.08.003.

42. J. T. Conway, "Geometric Efficiency for a Circular Detector and a Linear Source of Arbitrary Orientation and Position," *Nuclear Instruments and Methods in Physics Research Section A: Accelerators, Spectrometers, Detectors and Associated Equipment* 622, no. 3 (2010): 555–566, https://doi.org/10.1016/j.nima.2010.07.068.

43. M. I. Abbas, "Analytical Calculations of the Solid Angle Subtended by a Circular Disk Detector at Linear Sources," *Nuclear Instruments and Methods in Physics Research Section A: Accelerators, Spectrometers, Detectors and Associated Equipment* 904 (2018): 113–116, https://doi.org/10.1016/j.nima.2018.07.032.

44. H. R. Vega Carrillo, "Geometrical Efficiency for a Parallel Disk Source and Detector," *Nuclear Instruments and Methods in Physics Research Section A: Accelerators, Spectrometers, Detectors and Associated Equipment* 371, no. 3 (1996): 535–537, https://doi.org/10.1016/0168-9002(95)00998-1.

45. J. T. Conway, "Calculations for a Disk Source and a General Detector Using a Radiation Vector Potential," *Nuclear Instruments and Methods in Physics Research Section A: Accelerators, Spectrometers, Detectors and Associated Equipment* 589, no. 1 (2008): 20–33, https://doi.org/10.1016/j.nima.2008.02.017.

46. J. T. Conway, "Geometric Efficiency for a Circular Detector and a Ring Source of Arbitrary Orientation and Position," *Nuclear Instruments and Methods in Physics Research Section A: Accelerators, Spectrometers, Detectors and Associated Equipment* 640, no. 1 (2011): 99–109, https://doi.org/10.1016/j.nima.2011.03.014.

47. M. Prata, "Solid Angle Subtended by a Cylindrical Detector at a Point Source in Terms of Elliptic Integrals," *Radiation Physics and Chemistry* 67, no. 5 (2003): 599–603, https://doi.org/10.1016/S0969-806X(03)00144-0.

48. M. I. Abbas, "Analytical Calculations of the Solid Angles Subtended by a Well-Type Detector At Point and Extended Circular Sources," *Applied Radiation and Isotopes* 64, no. 9 (2006): 1048–1056, https://doi.org/10.1016/j.apradiso.2006.04.010.

49. M. I. Abbas, S. Hammoud, T. Ibrahim, and M. Sakr, "Analytical Formulae to Calculate the Solid Angle Subtended at an Arbitrarily Positioned Point Source by An Elliptical Radiation Detector," *Nuclear Instruments and Methods in Physics Research Section A: Accelerators, Spectrometers, Detectors and Associated Equipment* 771 (2015): 121–125, https://doi.org/10.1016/j.nima.2014.10.061.

50. G. Zhang and Z. Wei, "A Position-Distortion Model of Ellipse Centre for Perspective Projection," *Measurement Science and Technology* 14, no. 8 (2003): 1420, https://doi.org/10.1088/0957-0233/14/8/331.

51. Y. Sun, "Analysis for Center Deviation of Circular Target Under Perspective Projection," *Engineering Computations* 36, no. 7 (2019): 2403–2413, https://doi.org/10.1108/EC-09-2018-0431.

52. V. Gaudillière, G. Simon, and M. O. Berger, "Perspective-1-Ellipsoid: Formulation, Analysis and Solutions of the Camera Pose Estimation Problem From One Ellipse-Ellipsoid Correspondence," *International Journal of Computer Vision* 131, no. 9 (2023): 2446–2470.

53. J. A. Christian, "Optical Navigation Using Planet's Centroid and Apparent Diameter in Image," *Journal of Guidance, Control, and Dynamics* 38, no. 2 (2015): 192–204, https://doi.org/10.2514/1.G000872.

54. C. K. Chng, S. Mcleod, M. Rodda, and T. J. Chin, "Crater Identification by Perspective Cone Alignment," *Acta Astronautica* 224 (2024): 1–16, https://doi.org/10.1016/j.actaastro.2024.07.053.

55. D. Eberly, "Reconstructing an Ellipsoid From Its Perspective Projection onto a Plane," 2007. Last modified: February 14, 2019.

56. R. W. D. Nickalls, "Viète, Descartes and the Cubic Equation," *Mathematical Gazette* 90, no. 518 (2006): 203–208, https://doi.org/10.1017/S0025557200179598.

Appendix A

Roots of a Cubic Polynomial

Since the relevant characteristic polynomials in this study are presented as cubic polynomials, the corresponding solutions can be analytically derived. To specify the solutions, Equations (8) and (27) are transformed into the following simplified form.

$$\Lambda^3 + p\Lambda + q = 0, \tag{A1}$$

where

$$\Lambda = \lambda + \frac{A}{3}, \tag{A2}$$

$$p = B - \frac{A^2}{3}, \tag{A3}$$

$$q = C - \frac{AB}{3} + \frac{2A^3}{27}. \tag{A4}$$

When a cubic equation has three real roots, the triple angle formula of the trigonometric function can be used to find the solutions [56]. Alternatively, it is also possible to acquire the equivalent roots by Cardano's formula, as conducted in Conway's study [35]. However, since we are not strictly limited to the algebraic processes for evaluating the view factor, the former approach is applied for the description simplicity. The roots of the cubic equation of Equation (A1) are given by Equations (A5)–(A7), and the eigenvalues are given by Equation (A8).

$$\Lambda_1 = 2\sqrt{-\frac{p}{3}}\cos\left\{\frac{1}{3}\arccos\left(-\frac{3q}{2p}\sqrt{-\frac{3}{p}}\right)\right\}, \tag{A5}$$

$$\Lambda_2 = 2\sqrt{-\frac{p}{3}}\cos\left\{\frac{1}{3}\arccos\left(-\frac{3q}{2p}\sqrt{-\frac{3}{p}}\right) + \frac{2\pi}{3}\right\}, \tag{A6}$$

$$\Lambda_3 = 2\sqrt{-\frac{p}{3}}\cos\left\{\frac{1}{3}\arccos\left(-\frac{3q}{2p}\sqrt{-\frac{3}{p}}\right)+\frac{4\pi}{3}\right\}, \tag{A7}$$

$$\lambda_i = \Lambda_i - \frac{A}{3}, i = 1, 2, 3. \tag{A8}$$

The magnitude of these three eigenvalues has the following relationship: $\lambda_2 \le \lambda_3 \le \lambda_1$.